Two-temperature Brownian dynamics of a particle in a confining potential

Vincent Mancois,[1,2,3] Bruno Marcos,[4] Pascal Viot,[1,3] and David Wilkowski[1,2,5]
[1]*MajuLab, CNRS–Université de Nice-NUS-NTU International Joint Research Unit UMI 3654, Singapore*
[2]*PAP, School of Physical and Mathematical Sciences, Nanyang Technological University, 637371 Singapore*
[3]*Laboratoire de Physique Théorique de la Matière Condensée, Sorbonne Université, CNRS UMR 7600, 4 place Jussieu, 75252 Paris Cedex 05, France*
[4]*Université Côte d'Azur, CNRS, LJAD, 06108 Nice, France*
[5]*Centre for Quantum Technologies, National University of Singapore, 117543 Singapore*

(Received 26 January 2018; published 16 May 2018)

We consider the two-dimensional motion of a particle in a confining potential, subject to Brownian orthogonal forces associated with two different temperatures. Exact solutions are obtained for an asymmetric harmonic potential in the overdamped and underdamped regimes. For more general confining potentials, a perturbative approach shows that the stationary state exhibits some universal properties. The nonequilibrium stationary state is characterized with a nonzero orthoradial mean current, corresponding to a global rotation of the particle around the center. The rotation is due to two broken symmetries: two different temperatures and a mismatch between the principal axes of the confining asymmetric potential and the temperature axes. We confirm our predictions by performing a Brownian dynamics simulation. Finally, we propose to observe this effect on a laser-cooled atomic gas.

DOI: 10.1103/PhysRevE.97.052121

I. INTRODUCTION

When a system is in contact with two reservoirs of different temperatures or of different chemical potentials, the system does not relax to equilibrium but is driven toward a nonequilibrium stationary state. Moreover, for small systems, both the mean value and the fluctuations characterize the observables. Brownian particles driven by an external force provide paradigmatic models for studying fluctuation theorems and stochastic thermodynamics. When two heat reservoirs are in contact with a system, a conversion of fluctuations into directed transport and useful work can be observed. Derrida and Brunet [1] considered a one-dimensional stochastic model in contact with two thermostats in order to describe the time evolution of a hard rod whose extremities are in contact with two different thermostats. Visco [2] obtained the exact large deviation function of the work fluctuations of this model, showing that the fluctuation relations have a finite range of validity. (See also [3,4] for some generalizations.) Van den Broeck *et al.* [5] proposed an underdamped version of the Derrida and Brunet model and their analysis revealed that it contains the fundamental building blocks for thermal Brownian motors. (For reviews on Brownian motors, see [6,7]). More recently Murashita and Esposito [8] have revisited the one-dimensional stochastic models with multiple thermostats in the overdamped limit. They showed that it must be carefully considered, as one cannot simply derive the overdamped limit from the underdamped regime. Conversely, matching each reservoir to an independent degree of freedom of the particle, should ensure a proper overdamped limit. This latter situation, illustrated by two coupled particles in contact with two heat reservoirs, was recently experimentally and theoretically studied: Ciliberto *et al.* [9,10] measured the energy exchanged between two conductors kept at two different temperatures and linearly coupled. They analyzed experimental results in terms of two Brownian particles kept at different temperatures and coupled by an elastic force. Bérut *et al.* [11,12] measured the energy flux, the correlation functions and the probability distribution functions of a system of two particles hydrodynamically coupled at two different temperatures in optical traps. Finally, primacy of the coupling strength between particles in minimal thermal motors was demonstrated in [13]. (See also the recent review on experiments in stochastic thermodynamics [14]). Argun *et al.* [15] conducted an experiment with a single colloidal particle suspended in aqueous solution at room temperature and trapped in an elliptical optical potential, for which physical quantities were obtained from recorded particle trajectories. Chiang *et al.* [16] studied a simple stochastic electronic system featuring two resistor-capacitor circuits coupled by a third capacitor, which also represents an experimental realization of the overdamped version of the two-temperature model. Ryabov *et al.* [17,18] have considered the diffusion of a Brownian particle in a parabolic potential, in which the temperatures differed along the transversal and longitudinal directions.

In this paper, we consider the two-dimensional motion of a particle subject to two orthogonal Brownian forces of different temperatures, denoted T_x and T_y, respectively. Filliger and Reimann [19] initially proposed this simple model of an autonomous heat engine. This particle of mass m is also subjected to an external conservative force. The overdamped version of this model, in the case of an asymmetric harmonic potential, was previously studied by Dotsenko *et al.* [20]. They derived the nonequilibrium probability distribution function (PDF) of the positions and showed the presence of a nonzero current as long as the principal axes of the potential do not coincide with the temperature axes. We show that the emergence of this current is more general and is associated with the altogether two broken symmetries: two different

temperatures in two orthogonal directions and a mismatch between the temperature axes and the principal axes of the potential. Furthermore, we demonstrate that the macroscopic rotation is still present for an overdamped Brownian motion and for general confining potentials.

The article is organized as follows. In Sec. II, we consider the motion of a particle in an anisotropic harmonic trap for which we obtain exact expressions for PDF of positions and velocities as well as for the mean current. The latter is characterized by a mean angular velocity. In Sec. III, we address the general potential cases: performing a perturbative expansion with respect to a small temperature difference $(T_y - T_x)$ and a small asymmetry of the confining potential $U(x,y)$, characterized by a dimensionless parameter u. At the lowest order, the mean current velocity is proportional to $u(T_y - T_x)$. In Sec. IV, we perform numerical simulations of these models, both to confirm exact solutions obtained previously for a harmonic potential and to validate the perturbative approach for the general confining potentials. In Sec V, we discuss a possible experiment that may be carried out on a laser-cooled atomic gas. The rotation could be simply observed using standard time-of-flight (TOF) techniques.

II. HARMONIC POTENTIAL: EXACT SOLUTIONS

We consider a particle of mass m moving in a plane. This particle is subjected to a conservative force derived from a confining potential $U(x,y)$, a viscous linear force $-\eta\mathbf{v}$, and two stochastic forces $\sqrt{2T_i\eta}\xi_i(t)$. Here, η is the constant friction coefficient and T_i are the temperatures (expressed in units of energy) along the i axis where $i = x,y$. $\xi_i(t)$ are uncorrelated Gaussian white noises: $\langle\xi_i(t)\rangle = 0$ and $\langle\xi_i(t')\xi_j(t)\rangle = \delta(t - t')\delta_{ij}$, where $\delta(t)$ is the Dirac distribution and δ_{ij} is the Kronecker symbol.

A. Overdamped motion

1. Model A

We now assume that $U(x,y) = k(\frac{x^2+y^2}{2} + uxy)$ (with $|u| < 1$ for a confining potential), where k is the elasticity constant and u is a dimensionless parameter characterizing the potential anisotropy. More precisely, the principal axes of the potential are rotated by $\pi/4$ with respect to $\hat{x}$ and $\hat{y}$, the temperature axes, and $\sqrt{2u/(1-u)}$ is the eccentricity of the isopotentials. Figure 1 shows a contour plot of $U(x,y)$ with $k = 1$ and $u = 0.5$ with the two principal axes (red arrows) and the temperature axes (black arrows).

We first consider the overdamped motion in order to introduce the method used to solve the harmonic case [20]. The time evolution is given by the equations

$$\frac{dx}{dt} = -\frac{k}{\eta}(x + uy) + \sqrt{\frac{2T_x}{\eta}}\xi_x(t),$$
$$\frac{dy}{dt} = -\frac{k}{\eta}(y + ux) + \sqrt{\frac{2T_y}{\eta}}\xi_y(t). \quad (1)$$

The associated Fokker-Planck equation is given by

$$\frac{\partial P(x,y,t)}{\partial t} = -\nabla\cdot\mathbf{J}, \quad (2)$$

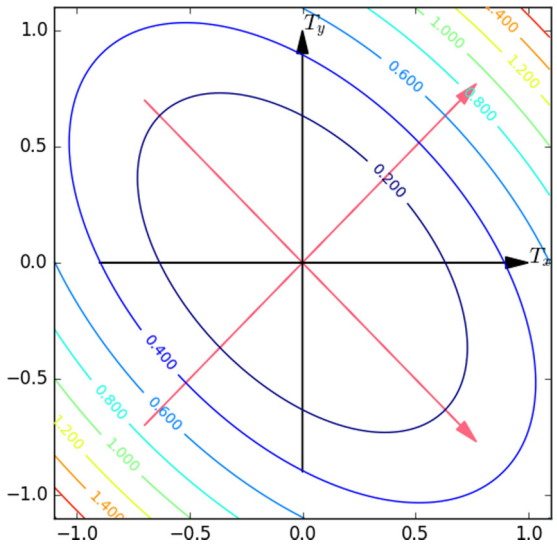

FIG. 1. Contour plot of $U(x,y)$ with $k = 1$ and $u = 0.5$. Red arrows correspond to the principal axes of the potential, and black arrows to the temperature axes.

where $\nabla = (\partial_x, \partial_y)$ and

$$\mathbf{J} = \begin{cases} J_x = -\frac{k}{\eta}(x + uy)P(x,y) - \frac{T_x}{\eta}\frac{\partial P}{\partial x}, \\ J_y = -\frac{k}{\eta}(y + ux)P(x,y) - \frac{T_y}{\eta}\frac{\partial P}{\partial y}. \end{cases} \quad (3)$$

To obtain the stationary position PDFs, we follow the method detailed in Appendix A. For this purpose, we introduce the 2×2 matrices A, B, and Ξ as

$$A = -\frac{k}{\eta}\begin{pmatrix} 1 & u \\ u & 1 \end{pmatrix}, \quad B = \frac{2}{\eta}\begin{pmatrix} T_x & 0 \\ 0 & T_y \end{pmatrix}, \quad (4)$$

and

$$\Xi = \frac{1}{2k(1-u^2)}\begin{pmatrix} 2T_x + (T_y - T_x)u^2 & -(T_x + T_y)u \\ -(T_x + T_y)u & 2T_y + (T_x - T_y)u^2 \end{pmatrix}. \quad (5)$$

The solution of Eq. (2) is the multivariate Gaussian distribution

$$P(\mathbf{z}) = \frac{1}{2\pi\sqrt{\mathrm{Det}(\Xi)}}\exp\left(-\frac{1}{2}(\mathbf{z} - \langle\mathbf{z}\rangle)^T\Xi^{-1}(\mathbf{z} - \langle\mathbf{z}\rangle)\right), \quad (6)$$

where $\mathbf{z}$ is a two-dimensional vector of components (x,y), $\mathbf{z}^T$ is its transpose vector, and $\langle\mathbf{z}\rangle$ its statistical average. Finally, the stationary PDF reads

$$P(x,y) = \frac{k\sqrt{1-u^2}e^{-(\gamma_1x^2+\gamma_2y^2+\gamma_3xy)}}{\pi\sqrt{4T_xT_y + u^2(T_y - T_x)^2}}, \quad (7)$$

where

$$\gamma_1 = k\frac{2T_y + u^2(T_x - T_y)}{4T_xT_y + u^2(T_x - T_y)^2}, \quad (8)$$

$$\gamma_2 = k\frac{2T_x + u^2(T_y - T_x)}{4T_xT_y + u^2(T_x - T_y)^2}, \quad (9)$$

$$\gamma_3 = k\frac{2u(T_x + T_y)}{4T_xT_y + u^2(T_x - T_y)^2}. \quad (10)$$

When $u = 0$, one recovers $P(x,y) \sim e^{-(kx^2/2T_x)-(ky^2/2T_y)}$, which corresponds to the equilibrium distribution of two decoupled oscillators. Integrating Eq. (7) over y or x, one obtains the marginal distributions $P(x)$ and $P(y)$, respectively, which have a Gaussian profile. The variances $\langle x^2\rangle$ and $\langle y^2\rangle$ are given by

$$\langle x^2\rangle = \frac{T_x + \frac{u^2}{2}(T_y - T_x)}{k(1-u^2)}, \tag{11}$$

$$\langle y^2\rangle = \frac{T_y + \frac{u^2}{2}(T_x - T_y)}{k(1-u^2)}, \tag{12}$$

with a cross correlation

$$\langle xy\rangle = -\frac{u(T_x + T_y)}{2k(1-u^2)}. \tag{13}$$

This term is nonzero only if $u \neq 0$.

The nonequilibrium stationary state is also characterized by a nonzero current probability $\mathbf{J} = \mathbf{v}P$ [21]. The angular velocity is defined as

$$\omega(t) = \frac{1}{r^2}(\mathbf{r}\times\mathbf{v}). \tag{14}$$

The mean angular velocity at long time is given by

$$\langle\omega\rangle = \lim_{t\to\infty}\frac{1}{t}\int_0^t dt'\omega(t'). \tag{15}$$

Assuming ergodicity of the system, the time average is equivalent to the ensemble average, therefore gving

$$\langle\omega\rangle = \int d^2\mathbf{r}\frac{1}{r^2}(\mathbf{r}\times\mathbf{v})P(\mathbf{r}). \tag{16}$$

Reexpressing in polar coordinates, one obtains

$$\langle\omega\rangle = \int_0^{2\pi} d\theta\int_0^{\infty} dr\, J_\theta(r,\theta), \tag{17}$$

with

$$J_\theta(r,\theta) = -\frac{kur\cos(2\theta)P}{\eta} - \frac{1}{2\eta r}(T_x+T_y)\frac{\partial P}{\partial\theta} - \frac{T_y - T_x}{2\eta}\left[\frac{\cos(2\theta)}{r}\frac{\partial P}{\partial\theta} + \sin(2\theta)\frac{\partial P}{\partial r}\right]. \tag{18}$$

The position PDF $P(r,\theta)$ is then given by

$$P(r,\theta) = \frac{k\sqrt{1-u^2}e^{-[\gamma_+ + \gamma_-\cos(2\theta)+u\gamma_+\sin(2\theta)]r^2}}{\pi\sqrt{4T_xT_y + u^2(T_y-T_x)^2}}, \tag{19}$$

with

$$\gamma_+ = k\frac{T_x+T_y}{4T_xT_y + u^2(T_x-T_y)^2}, \tag{20}$$

$$\gamma_- = k\frac{(1-u^2)(T_y-T_x)}{4T_xT_y + u^2(T_x-T_y)^2}. \tag{21}$$

By inserting Eq. (19) into Eq. (18), the orthoradial current $J_\theta(r,\theta)$ reads

$$J_\theta(r,\theta) = \frac{u(T_y-T_x)r}{\eta}[\gamma_+ + \gamma_-\cos(2\theta) + u\gamma_+\sin(2\theta)] \times P(r,\theta). \tag{22}$$

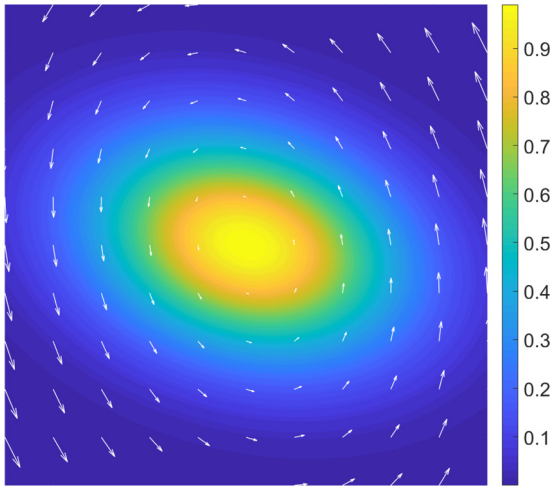

FIG. 2. Density plot of the position PDF $P(x,y)$ and vector field of the orthoradial velocity (white arrows), $v_\theta(r,\theta)$, for a harmonic potential with $u = 0.2$, $T_x = 1$, and $T_y = 2$. The color bar displays the relative density scale.

Finally, the mean angular velocity is given by

$$\langle\omega\rangle = \frac{k}{\eta}u(T_y-T_x)\sqrt{\frac{1-u^2}{4T_xT_y + u^2(T_x-T_y)^2}}. \tag{23}$$

Higher moments of $\langle\omega\rangle$ can also be calculated,

$$\langle\omega^n\rangle = k\left(\frac{u(T_y-T_x)}{\eta}\right)^n\sqrt{\frac{1-u^2}{4T_xT_y + u^2(T_x-T_y)^2}} \times\int_0^{2\pi}\frac{d\theta}{2\pi}[\gamma_+ + \gamma_-\cos(2\theta) + u\gamma_+\sin(2\theta)]^{n-1} \tag{24}$$

which gives the following variance:

$$\langle\omega^2\rangle - \langle\omega\rangle^2 = k\left(\frac{u(T_y-T_x)}{\eta}\right)^2\frac{1-u^2}{4T_xT_y + u^2(T_x-T_y)^2} \times\left[\frac{T_x+T_y}{\sqrt{4T_xT_y + u^2(T_x-T_y)^2}} - 1\right]. \tag{25}$$

All moments also vanish when $u = 0$ or $T_y = T_x = 0$, which means a complete absence of global rotation if the two symmetries are not broken.

Figure 2 shows the density plot of the position PDF, $P(x,y)$, and the vector field of the orthoradial velocity, $v_\theta(r,\theta) = J_\theta(r,\theta)/P(r,\theta)$, for a harmonic potential with an asymmetry parameter $u = 0.2$ and two temperatures $T_y = 2T_x = 1$. The particle density displays a maximum at the center, whereas $v_\theta(r,\theta)$ increases linearly with the distance r.

We see that a nonzero current requires two broken symmetries: two different temperatures along the orthogonal axes which do not match the principal axes of the potential.

2. *Model B*

In order to show that the nonzero current does not originate from the anisotropy of the potential, but from the mismatch between the principal axes of the potential and the temperature axes, one considers a second model where the particle evolves in a potential $U(x,y) = k(\frac{x^2+a^2y^2}{2} + uxy)$. Stable potentials

require $|a| > |u|$. By using the same method, one obtains an exact solution of the stationary probability $P(x,y)$, which reads

$$P(x,y) = \frac{k(1+a^2)\sqrt{a^2-u^2}e^{-(\gamma_1' x^2+\gamma_2' y^2+\gamma_3' xy)}}{\pi\sqrt{(1+a^2)^2T_xT_y+u^2(T_y-T_x)^2}}, \tag{26}$$

where

$$\gamma_1' = k\frac{(1+a^2)[T_y(1+a^2)+u^2(T_x-T_y)]}{2[(1+a^2)^2T_xT_y+u^2(T_x-T_y)^2]}, \tag{27}$$

$$\gamma_2' = k\frac{(1+a^2)[2T_x+u^2(T_y-T_x)]}{2[(1+a^2)^2T_xT_y+u^2(T_x-T_y)^2]}, \tag{28}$$

$$\gamma_3' = k\frac{(1+a^2)u(a^2T_x+T_y)}{(1+a^2)^2T_xT_y+u^2(T_x-T_y)^2}. \tag{29}$$

Inserting Eq. (26) into Eq. (17), one obtains the mean angular velocity:

$$\langle\omega\rangle = \frac{k}{\eta}u(T_y-T_x)\sqrt{\frac{a^2-u^2}{(1+a^2)^2T_xT_y+u^2(T_x-T_y)^2}}. \tag{30}$$

For an anisotropic potential where the confinement is different along the two temperature axes, it is noticeable that a nonzero mean angular velocity is still proportional to the product $u(T_y - T_x)$, which means that the joint effect of the temperature difference and of the anisotropy of the potential whose principal axes are different from temperature axes leads to a global rotation. The effect of this anisotropy along the y axis only modifies the amplitude of angular velocity, but is not responsible for the global rotation [see Eq. (30)]. The principal axes of the anisotropic potential are rotated by an angle α, such that

$$\tan(2\alpha) = \frac{2u}{1-a^2} \tag{31}$$

which varies continuously from 0 to $\frac{1}{2}\arctan(\frac{2^*a}{1-a^2})$ when u goes from 0 to a.

B. Underdamped motion

Returning to the previous anisotropic potential $U(x,y) = k(\frac{x^2+y^2}{2} + uxy)$, we now consider an underdamped motion (see also [22]). The equations of motion of a particle are given by

$$\begin{aligned}
\frac{dv_x}{dt} &= -\frac{1}{m}\frac{\partial U(x,y)}{\partial x} - \frac{\eta}{m}v_x + \sqrt{\frac{2\eta T_x}{m^2}}\xi_x(t),\\
\frac{dv_y}{dt} &= -\frac{1}{m}\frac{\partial U(x,y)}{\partial y} - \frac{\eta}{m}v_y + \sqrt{\frac{2\eta T_y}{m^2}}\xi_y(t),\\
\frac{dx}{dt} &= v_x, \quad \frac{dy}{dt} = v_y.
\end{aligned} \tag{32}$$

The Kramers-Fokker-Planck equation corresponding to the underdamped motion, is expressed as

$$\frac{\partial P(x,y,v_x,v_y,t)}{\partial t} = -\nabla\cdot\mathbf{J}, \tag{33}$$

where $\nabla = (\partial_x, \partial_y, \partial_{v_x}\partial_{v_y})$ and

$$\mathbf{J} = \begin{cases}
J_x = v_xP,\\
J_y = v_yP,\\
J_{v_x} = \left(-\frac{1}{m}\frac{\partial U(x,y)}{\partial x} - \eta\frac{v_x}{m}\right)P - \frac{\partial}{\partial v_x}\left(\frac{\eta T_x}{m^2}P\right),\\
J_{v_y} = \left(-\frac{1}{m}\frac{\partial U(x,y)}{\partial y} - \eta\frac{v_y}{m}\right)P - \frac{\partial}{\partial v_y}\left(\frac{\eta T_y}{m^2}P\right).
\end{cases} \tag{34}$$

The stationary PDF now depends on the variables x, y, v_x, and v_y which are defined as components of a four-component vector $\mathbf{z}$. The associated matrices A and B are given by

$$\begin{aligned}
A &= \frac{1}{m}\begin{pmatrix} 0 & 0 & m & 0\\ 0 & 0 & 0 & m\\ -k & -ku & -\eta & 0\\ -ku & -k & 0 & -\eta\end{pmatrix},\\
B &= \frac{\eta}{m^2}\begin{pmatrix} 0 & 0 & 0 & 0\\ 0 & 0 & 0 & 0\\ 0 & 0 & 2T_x & 0\\ 0 & 0 & 0 & 2T_y\end{pmatrix}.
\end{aligned} \tag{35}$$

Introducing a dimensionless viscosity $\eta' = \eta/\sqrt{km}$ and solving Eq. (A3), one obtains

$$\Xi = \begin{pmatrix}
\frac{2\eta'^2T_x+u^2(T_x+T_y)+\eta'^2(T_y-T_x)}{2k(\eta'^2+u^2)(1-u^2)} & -\frac{u(T_x+T_y)}{2k(1-u^2)} & 0 & -\frac{\eta'(T_x-T_y)u}{2\sqrt{km}(\eta'^2+u^2)}\\
\frac{-u(T_x+T_y)}{2k(1-u^2)} & \frac{2\eta'^2T_y+u^2(T_x+T_y)+\eta'^2(T_x-T_y)}{2k(\eta'^2+u^2)(1-u^2)} & \frac{\eta'(T_x-T_y)u}{2\sqrt{km}(\eta'^2+u^2)} & 0\\
0 & \frac{\eta'(T_x-T_y)u}{2\sqrt{km}(\eta'^2+u^2)} & \frac{2T_x\eta'^2+(T_x+T_y)u^2}{2m(\eta'^2+u^2)} & 0\\
-\frac{\eta'(T_x-T_y)u}{2\sqrt{km}(\eta'^2+u^2)} & 0 & 0 & \frac{2T_y\eta'^2+(T_x+T_y)u^2}{2m(\eta'^2+u^2)}
\end{pmatrix}. \tag{36}$$

Inverting Ξ leads to the probability distribution $P(x,y,v_x,v_y)$. The marginal probability distributions, namely, the position, P_x, P_y and velocity P_{v_x}, P_{v_y} PDFs can be easily calculated. The position PDFs P_x, P_y are given by

$$P_z(z) = \sqrt{\frac{1}{2\pi T_{ze}}}\exp\left(-\frac{z^2}{2T_{ze}}\right), \tag{37}$$

where $z = x, y$.

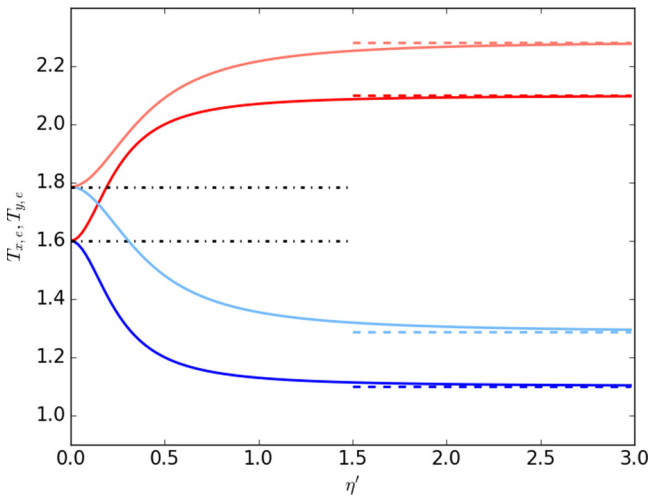

FIG. 3. Effective temperatures T_{xe} and T_{ye} of the position PDFs versus the viscosity η for $T_x = 1$, $T_y = 2$ and $u = 0.25$ (lower curves) and $u = 0.4$ (upper curves). The full lines correspond to the temperatures along the directions $\hat{x}$ (blue) and $\hat{y}$ (red). The dashed lines give the high friction limit, where the two effective temperatures are larger and smaller than T_x and T_y. The dashed-dotted lines indicate the zero friction limit, respectively.

T_{xe} is the effective temperature of P_x given by

$$T_{xe} = \frac{\eta'^2 T_x + \frac{u^2}{2}[\eta'^2(T_y - T_x) + (T_x + T_y)]}{(1-u^2)(\eta'^2 + u^2)}. \tag{38}$$

A similar expression for T_{ye} is obtained:

$$T_{ye} = \frac{\eta'^2 T_y + \frac{u^2}{2}[\eta'^2(T_x - T_y) + (T_x + T_y)]}{(1-u^2)(\eta'^2 + u^2)}. \tag{39}$$

When $\eta' \gg 1$, Eqs. (38) and (39) go to the overdamped limit given by Eqs. (11) and (12). Conversely, when $\eta' \to 0$, the two effective temperatures become equal, $T_{xe} = T_{ye} = \frac{T_x + T_y}{2(1-u^2)}$.

Figure 3 shows how T_{xe} and T_{ye} depend on the dimensionless viscosity η' for $T_x = 1$ and $T_y = 2$ (full lines). Note that effective temperatures T_{xe} and T_{ye}, which start from the same value $(T_x + T_y)/2(1-u^2)$, respectively decrease and increase toward their asymptotic values, $T_{xe}(\infty)$ and $T_{ye}(\infty)$. In other words, at low viscosity, the widths of the position PDF are given by the mean temperature of both directions [up to a $(1-u^2)^{-1}$ factor]. When the dimensionless viscosity increases, the effective temperatures go rapidly toward the asymptotic values (which are independent of the viscosity). It may be noted that the effective temperatures along each direction are different from T_x and T_y, respectively. Another feature, shown in Fig. 3, is the interplay between u and η'. Moreover, the inflection point, located at $\eta' \approx u/\sqrt{3}$, marks the crossover between overdamped and underdamped regimes.

Figure 4 shows the position PDFs, P_x and P_y for two temperatures T_x and T_y and $\eta' = 1$ (full curves). The dashed curves represent the underdamped Langevin simulation (see Sec. IV for more details) and closely agree with the exact expressions, Eq. (37).

We now consider the velocity PDFs for which one obtains an exact expression for the harmonic model. Integrating $P(x, y, v_x, v_y)$ over the position and one velocity component,

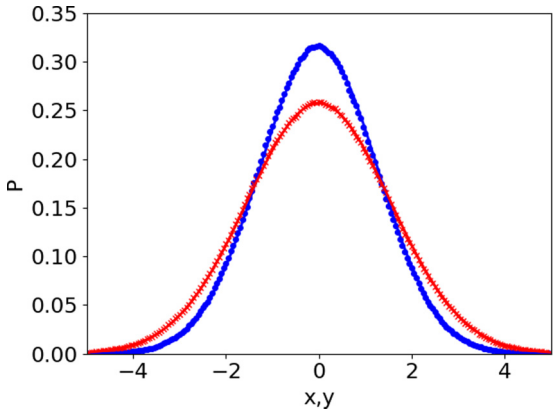

FIG. 4. Stationary position PDF $P(x)$ (blue) and $P(y)$ (red) for an asymmetric harmonic potential ($u = 0.5$), a dimensionless viscosity $\eta' = 1$, with $T_x = 1$ and $T_y = 2$.

it is easy to show that the velocity PDFs keep also a Gaussian shape with an effective temperature $T_{v_x e}$ and $T_{v_y e}$, respectively:

$$T_{v_x e} = \frac{2T_x\eta'^2 + u^2(T_x + T_y)}{2(u^2 + \eta'^2)}, \tag{40}$$

$$T_{v_y e} = \frac{2T_y\eta'^2 + u^2(T_x + T_y)}{2(u^2 + \eta'^2)}. \tag{41}$$

As expected, when $\eta' \to \infty$, one recovers that $T_{v_x e} = T_x$ and $T_{v_y e} = T_y$ irrespective of u, which means that the velocity distribution is independent of the potential in the high friction limit. Conversely, when $\eta' \to 0$, the two effective temperatures, $T_{v_x e}$ and $T_{v_y,e}$, go to the same limit $(T_x + T_y)/2$.

Figure 5 shows $T_{v_x,e}$ and $T_{v_y,e}$ as a function of viscosity for two values of the asymmetry parameter $u = 0.25, 0.4$. As previously observed for the effective temperatures $T_{x,e}$ and $T_{y,e}$ of the position PDFs, the asymptotic values of the high friction

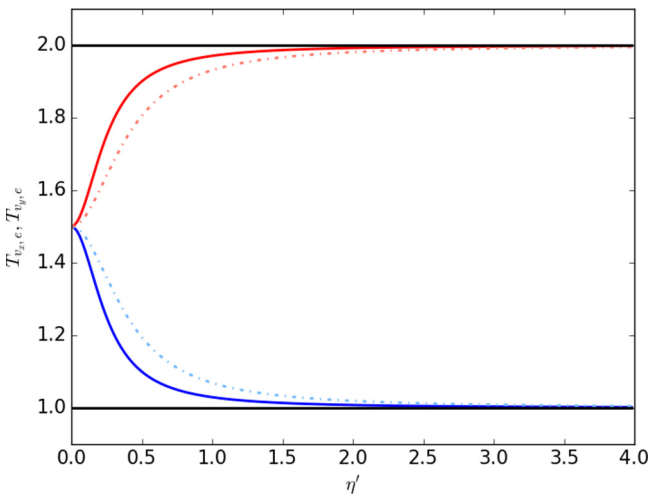

FIG. 5. Effective temperatures $T_{v_x,e}$ and $T_{v_y,e}$ of the velocity PDFs for an asymmetric harmonic potential with a viscosity $\eta = 1$, $T_x = 1$, $T_y = 2$ and for two values of the asymmetry parameter $u = 0.25$ (full curves) and $u = 0.4$ (dot-dashed curves). The magenta lines give the $\eta' \to +\infty$ limit.

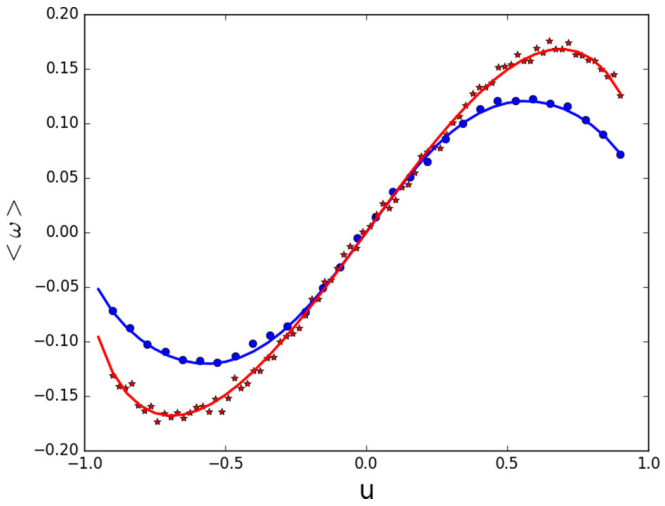

FIG. 6. Mean angular velocity $\langle\omega\rangle$ (in rad s^{-1}) as a function of the asymmetry parameter u for two different viscosities $\eta' = 1,5$, when $T_x = 1$, $T_y = 2$ (circles and stars). The full curves correspond to the exact expression, Eq. (44). The dots correspond to the simulation results.

limit are rapidly reached ($\eta' > 2$). However, although $T_{x,e}$ and $T_{y,e}$ goes to asymptotic values which depend on the asymmetry parameter u and on the two temperatures T_x and T_y, $T_{v_x,e}$ and $T_{v_y,e}$ instead go to T_x and T_y, respectively.

Whereas the stationary positions and velocities PDFs are symmetric and have a Gaussian shape, the particle motion exhibits a mean rotation velocity. The mean angular velocity is given by

$$\langle\omega\rangle = \int d^2\mathbf{r} \int d^2\mathbf{v} \frac{1}{r^2}(\mathbf{r}\times\mathbf{v})P(\mathbf{r},\mathbf{v}). \tag{42}$$

Converting the above expression to polar coordinates gives

$$\langle\omega\rangle = \int dv_r \int dv_\theta \int d\theta \int dr\, v_\theta P(r,\theta,v_r,v_\theta). \tag{43}$$

After some calculation, one obtains the expression

$$\langle\omega\rangle = \frac{ku(T_y - T_x)\sqrt{1-u^2}}{\eta\sqrt{[4T_x T_y + u^2(T_x - T_y)^2] + \left(\frac{u^4}{\eta'^4} + 2\frac{u^2}{\eta'^2}\right)(T_y + T_x)^2}}. \tag{44}$$

In the overdamped limit ($\eta' \to \infty$) one recovers Eq. (23). In the opposite limit $\eta' \to 0$, the mean angular velocity decreases to zero as the inverse of the particle mass.

Figure 6 shows the evolution of $\langle\omega\rangle$ as a function of the asymmetry parameter u for two values $\eta' = 1,5$. The full curves correspond to Eq. (44). As previously observed with the effective temperatures, shown in Figs 3 and 5, for $\eta' > 3$, the mean angular velocity matches the exact expression corresponding to the high-friction limit. Note that for a given value u, the friction coefficient has a weaker impact than the asymmetry parameter u.

We have shown that the two-temperature model has a stationary solution with a nonzero current when both the potential is asymmetric and the temperatures are different. One notes that the current is maximum in the overdamped situation.

III. WEAK ASYMMETRIC POTENTIAL

We now consider the overdamped motion of a particle of mass m in a weak asymmetric potential $U(r,\theta) = U_0(r) + uU_1(r,\theta)$, where $u \ll 1$ is a small dimensionless parameter and $U_1(r,\theta) \leqslant U_0(r)$ when r is large. Moreover, both temperatures are taken to be close in order to perform a perturbative expansion of the Fokker-Planck equation. One defines the mean temperature $T = (T_x + T_y)/2$. The two temperatures along the two axes are then expressed as $T_x = T(1 - \alpha/2)$ and $T_y = T(1 + \alpha/2)$, and $|\alpha| \ll 1$ is a small dimensionless parameter. Using Eq. (3) and expressing the current in polar coordinates, the stationary solution $P(r,\theta)$ satisfies

$$\frac{1}{r}\frac{\partial(rJ_r)}{\partial r} + \frac{1}{r}\frac{\partial J_\theta}{\partial\theta} = 0, \tag{45}$$

where the radial and orthoradial currents, J_r and J_θ, are the sum of the two contributions

$$J_{r,\theta} = J^1_{r,\theta} + J^2_{r,\theta}, \tag{46}$$

where

$$J^1_r(r,\theta) = -\frac{P}{\eta}\frac{\partial U}{\partial r} - \frac{T}{\eta}\frac{\partial P}{\partial r}, \tag{47}$$

$$J^1_\theta(r,\theta) = -\frac{P}{\eta r}\frac{\partial U}{\partial\theta} - \frac{T}{\eta r}\frac{\partial P}{\partial\theta} \tag{48}$$

and

$$J^2_r(r,\theta) = -\frac{\alpha T}{2\eta}\left(-\cos(2\theta)\frac{\partial P}{\partial r} + \frac{\sin(2\theta)}{r}\frac{\partial P}{\partial\theta}\right), \tag{49}$$

$$J^2_\theta(r,\theta) = -\frac{\alpha T}{2\eta}\left(\sin(2\theta)\frac{\partial P}{\partial r} + \frac{\cos(2\theta)}{r}\frac{\partial P}{\partial\theta}\right). \tag{50}$$

J^1 and J^2 are the currents associated with the mean temperature and with the temperature difference along the two axes, respectively. When $\alpha = 0$, the stationary solution of the Fokker-Planck equation is the equilibrium distribution $P^u_0(r,\theta) \propto e^{-[U_0(r)+uU_1(r,\theta)]/T}$, where the associated current vanishes.

We now propose the following ansatz for the stationary distribution

$$P(r,\theta) = P^u_0(r,\theta)P_1(r,\theta), \tag{51}$$

which gives

$$J^1_r(r,\theta) = -\frac{T P^u_0(r,\theta)}{\eta}\frac{\partial P_1(r,\theta)}{\partial r},$$
$$J^1_\theta(r,\theta) = -\frac{T P^u_0(r,\theta)}{\eta r}\frac{\partial P_1(r,\theta)}{\partial\theta}. \tag{52}$$

Inserting Eq. (52) into Eq. (45), one finally obtains

$$P^u_0(r,\theta)\Delta P_1(r,\theta) + \vec{\nabla}P^u_0(r,\theta)\cdot\vec{\nabla}P_1(r,\theta) = -\frac{\eta}{T}\vec{\nabla}\cdot\vec{J}^2. \tag{53}$$

Assuming that $P_1(r,\theta) \propto \exp[-\alpha f(r,\theta,u,\alpha)]$, and performing a first-order expansion in α (and a zeroth-order expansion in

u), one has

$$\Delta P_1(r,\theta) = -\alpha P_1(r,\theta)\Delta f(r,\theta) + O(\alpha^2), \tag{54}$$

$$\vec{\nabla} P_0^u(r,\theta)\cdot\vec{\nabla} P_1(r,\theta) = \frac{\alpha}{T} P_0^0(r) P_1(r,\theta)\frac{\partial U_0(r)}{\partial r}\frac{\partial f(r,\theta)}{\partial r} + O(\alpha^2), \tag{55}$$

and

$$\vec{\nabla}\cdot\vec{J}^2 = \frac{\alpha\,\cos(2\theta)}{2\eta} P_0^0(r) P_1(r,\theta)\left[\frac{1}{r}\frac{\partial}{\partial r}\left(r\frac{\partial U_0(r)}{\partial r}\right) - \frac{1}{T}\left(\frac{\partial U_0(r)}{\partial r}\right)^2 - \frac{2}{r}\frac{\partial U_0(r)}{\partial r}\right] + O(\alpha^2). \tag{56}$$

Therefore, the function $f(r,\theta)$ satisfies the partial differential equation

$$\Delta f(r,\theta) - \frac{1}{T}\frac{\partial U_0(r)}{\partial r}\frac{\partial f(r,\theta)}{\partial r} = \frac{\cos(2\theta)}{2T}\left[\frac{1}{r}\frac{\partial}{\partial r}\left(r\frac{\partial U_0(r)}{\partial r}\right) - \frac{1}{T}\left(\frac{\partial U_0(r)}{\partial r}\right)^2 - \frac{2}{r}\frac{\partial U_0(r)}{\partial r}\right]. \tag{57}$$

Assuming that $f(r,\theta) = \cos(2\theta) g(r)$, one obtains a differential equation for $g(r)$.

$$\frac{d^2 g(r)}{dr^2} + \frac{1}{r}\frac{dg(r)}{dr} - 4\frac{g(r)}{r^2} - \frac{1}{T}\frac{\partial U_0(r)}{\partial r}\frac{dg(r)}{dr} = \frac{1}{2T}\left[\frac{1}{r}\frac{\partial}{\partial r}\left(r\frac{\partial U_0(r)}{\partial r}\right) - \frac{1}{T}\left(\frac{\partial U_0(r)}{\partial r}\right)^2 - \frac{2}{r}\frac{\partial U_0(r)}{\partial r}\right]. \tag{58}$$

The analytical solution of the differential cannot be obtained in general. However, assuming that $U_0(r) \sim r^p$ (with $p \geqslant 2$) when $r \to \infty$, one obtains that the asymptotic behavior of $g(r)$ is $g(r) \sim U_0(r)/(2T)$. A solution exists for the harmonic potential where $g(r) = kr^2/(4T)$. The probability distribution is then given by

$$P(r,\theta) \propto \exp\left\{-\frac{kr^2}{2T}\left[1 + u\,\sin(2\theta) + \frac{\alpha}{2}\cos(2\theta)\right]\right\}, \tag{59}$$

which corresponds to the lowest-order expansion in u and α of Eq. (19). Hence, the mean angular velocity is given by $\langle\omega\rangle \propto \alpha u k T/\eta$.

Similarly, we now show that the ansatz gives the leading behavior of the mean angular velocity. Inserting $P(r,\theta) \propto \exp[-(U_0(r) + uU_1(r,\theta)]/T - \alpha\cos(2\theta) g(r)))$ into Eq. (48), one obtains

$$J_\theta^1(r,\theta) = -\frac{2T\alpha}{\eta r} g(r)\sin(2\theta) P(r,\theta). \tag{60}$$

The Fourier series of the anisotropic part of the potential is $U_1(r,\theta) = \sum_{n\geqslant 2}[a_n(r)\cos(n\theta) + b_n(r)\sin(n\theta)]$. Because the principal axes of the potential mismatch of the temperature axes, this implies that $b_2(r)$ is nonzero ([or at least a single $b_n(r)$, $n \geqslant 2$, is nonzero]. Performing an expansion in u and α of Eq. (59), one obtains that the integral of $J^1(r,\theta)$ over θ is proportional to $\alpha u T$.

Similarly, inserting the ansatz for $P(r,\theta)$ into Eq. (50), the leading term of the current is given by

$$J_\theta^2(r,\theta) = \frac{\alpha}{2\eta}\left(\sin(2\theta)\frac{\partial U_0(r,\theta)}{\partial r}\right) P(r,\theta). \tag{61}$$

The integration of $J_\theta^2(r,\theta)$ provides a second contribution to $\langle\omega\rangle$, also proportional to $\alpha u T$. Note that when $g(r) = \frac{r}{4T}\frac{\partial U_0(r)}{\partial r}$ the two contributions vanish. For this case which corresponds to the harmonic potential, the orthogonal current must be calculated to the next order, which is proportional to $u\alpha T/\eta$. One then recovers results obtained in Sec. II, where the mean angular velocity is proportional to $u\alpha T/\eta$. Finally, we have shown that the mean angular velocity is proportional to $u\alpha T/\eta$ (for $u,\alpha \ll 1$) which confirms the existence of the mean current linked to the double symmetry breaking.

IV. SIMULATION

We performed a stochastic simulation of a particle in the underdamped situation in order to test the results obtained in the high friction limit. To solve the stochastic differential equation in the underdamped situation, we implement a Verlet-like algorithm which has the property of using one random number per time step [23] (see Appendix B). Each run is performed with a total reduced elapsed time 3000. Position and velocity PDFs are monitored in the stationary regime. To obtain reliable statistics, one considers the probability distribution along each axis instead of two-dimensional probability distribution.

We first consider the harmonic potential: all monitored quantities such as position PDFs, velocity PDFs, and the mean angular velocity match the exact results for any value of the viscosity. In particular, we recover the overdamped limit very rapidly when $\eta' > 3$.

As discussed above, no exact expression is obtained even for a spherical potential except the harmonic one. We first simulate the model for $U(x,y) = (x^2+y^2)^2/4 + uxy$. Figure 7 displays the asymmetry of the potential for $u = 3$ and $u = -3$. The mean angular velocity is plotted as a function of the asymmetry parameter u (see Fig. 8) for different values of $T_y = 2,1.5,1.2,0.8,0.5$ and $T_x = 1$. These values correspond to $\alpha = 1,0.5,0.2,-0.2,-0.5$ and $T = 1.5,1.1,0.9,0.75$, respectively. The perturbative analysis of Sec. III predicts that the mean angular velocity is proportional to $\alpha u T$ when $u,\alpha \ll 1$. Figure 8 shows the reduced mean angular velocity ω as a function of u (for different α), and we observe that all the

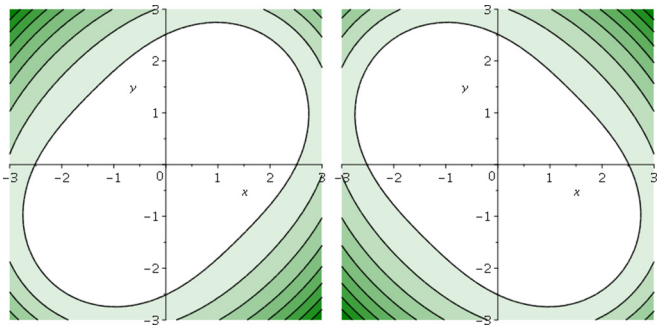

FIG. 7. Contour plot of the potential $U(x,y) = (x^2+y^2)^2/4 + uxy$ for $u = 3$ (left) and $u = -3$ (right).

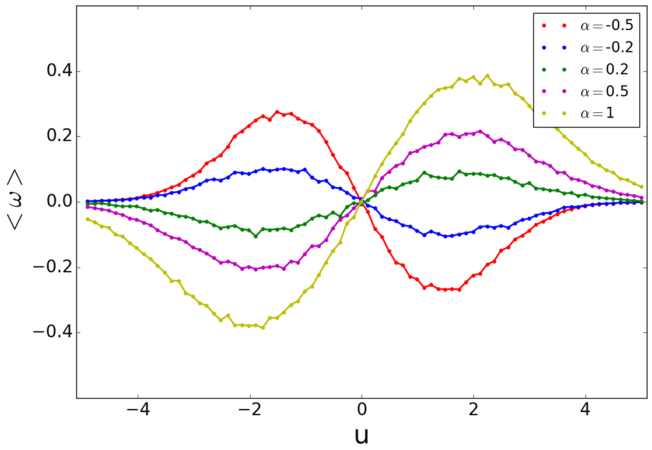

FIG. 8. Reduced mean angular velocity versus the asymmetry parameter u for a potential $U(x,y) = (x^2+y^2)^2/4 + uxy$, with different values of α.

curves collapse for small values of u (see Fig. 9). For $u = 0$, no mean current exists. For $u > 1.5$, a nonlinear dependence on u appears and two extreme values of the mean angular velocity exist for $u \simeq \pm 2$. In addition, the intensity of the mean angular velocity is increased compared to the harmonic case.

V. OBSERVATION ON COLD ATOMS

Cold atom experiments can deal with intensity or laser detuning imbalance during the cooling phase, leading to different temperatures along the different cooling axes. By adding a two-dimensional optical dipole trap, one can tailor the asymmetric parameter u at will. Breaking the two symmetries in this case, we raise the question to what extent this thermal rotation can be observed. The rotation of atomic clouds has been previously reported in the context of a beam-misaligned vortex trap [24,25] and more recently using synthetic Lorentz forces [26–28]. As opposed to those previous studies where the rotation is due to a net mean radiation pressure force, our proposal is based on a stochastic force with zero mean value.

We compute $\langle\omega\rangle$ for optical molasses, in the presence of an optical dipole trap using a semiclassical approach of laser cooling (see, for example, [29]). For simple experimental implementation, we consider a two-dimensional laser cooling where all laser beams have the same frequency detuning δ with respect to an atomic transition but with different laser intensities I_x and I_y, respectively, along the x axis and y axis. We can then define the saturation parameter $s_i = (I_i/I_s)/(1 + 4\delta^2/\Gamma^2)$, where I_s is the saturation intensity of the atomic transition and Γ is the atomic linewidth and $i = x, y$. In what follows, we consider the low saturation limit, namely, $s_i \ll 1$, so we can sum up the individual contributions of each laser beam to the total radiation pressure force (mean and fluctuating parts). The expansion for the viscous force (mean component) along the i axis reads

$$\mathbf{F}_i = -\eta_i \mathbf{v}, \quad \eta_i = -4\hbar k^2 s_i \frac{2\delta/\Gamma}{1 + (2\delta/\Gamma)^2}, \tag{62}$$

where k the wave vector of the laser beams and $\hbar$ the Planck constant.

The diffusion constant (fluctuating component), along the x axis reads

$$D_x = \tfrac{1}{4}\hbar^2 k^2 \Gamma(s_x + s_y) + \tfrac{1}{2}\hbar^2 k^2 \Gamma s_x. \tag{63}$$

The first term on the right-hand side of Eq. (63) comes from the photon spontaneous emission events (isotropic radiation pattern), whereas the second term is due to the laser photon absorption events. A similar expression is found along the y axis by swapping subscripts x and y in Eq. (63). Additionally, we assume $\eta = (\eta_x + \eta_y)/2$ in order to simplify the calculation. More precisely, we could set $\eta_x = \eta_y$ and $D_x \neq D_y$ by choosing different frequencies detuning and different intensities.

The temperatures along each direction $i = x, y$ are given by the Einstein-Smoluchowski relation:

$$T_i = \frac{D_i}{\eta}. \tag{64}$$

The presence of an asymmetric optical dipole trap $U(x,y) = \frac{m\omega_T^2}{2}(x^2 + y^2 + 2uxy)$, leads to the second broken symmetry. According to Eq. (44) the mean angular frequency reads

$$\langle\omega\rangle = \frac{m(\hbar k\omega_T)^2}{2\eta^2} u(s_y - s_x)\sqrt{\frac{1-u^2}{4T_xT_y + u^2(T_x - T_y)^2}}. \tag{65}$$

The scheme could not be implemented on standard alkaline atoms where broad transitions usually lead to Doppler temperatures higher than the potential depth. In contrast, narrow intercombination lines of alkaline-earth-metal atoms are favorable to such experiments. For instance, cooling of bosonic strontium 88 on the intercombination line $^1S_0 \rightarrow {}^3P_1$ of linewidth $\Gamma/2\pi = 7.5$ kHz, leads to temperatures in the microkelvin range compatible with usual dipole trap depth [30,31]. For an illustrative and realistic example, we take a dipole trap frequency of $\omega_T = 250$ Hz, saturation parameters $\{\frac{I_x}{I_s}, \frac{I_y}{I_s}\} = 1,4$, and a detuning $\delta = -3$. We choose a trap anisotropy parameter $u = 0.4$. Our model gives $T_x = 0.39\ \mu$K, $T_y = 0.72\ \mu$K, and a mean angular velocity of 15 Hz. Additionally, the inverse quality factor (dimensionless viscosity) η' is close to 2, indicating an overdamped dynamic. Figure 10 displays a simple TOF experiment to visualize the effect. After stirring the atoms, we release them from the trap and follow their ballistic expansion along x and y. The clockwise (upper) and counterclockwise (lower) cases

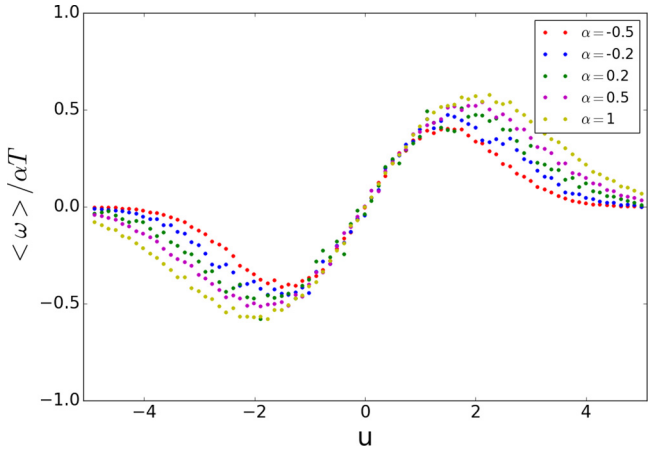

FIG. 9. Rescaled mean angular velocity $\omega/(\alpha T)$ versus the asymmetry parameter u for the potential $U(x,y) = (x^2+y^2)^2/4 + uxy$ and $\alpha = 1, 0.5, 0.2, -0.2, -0.5$.

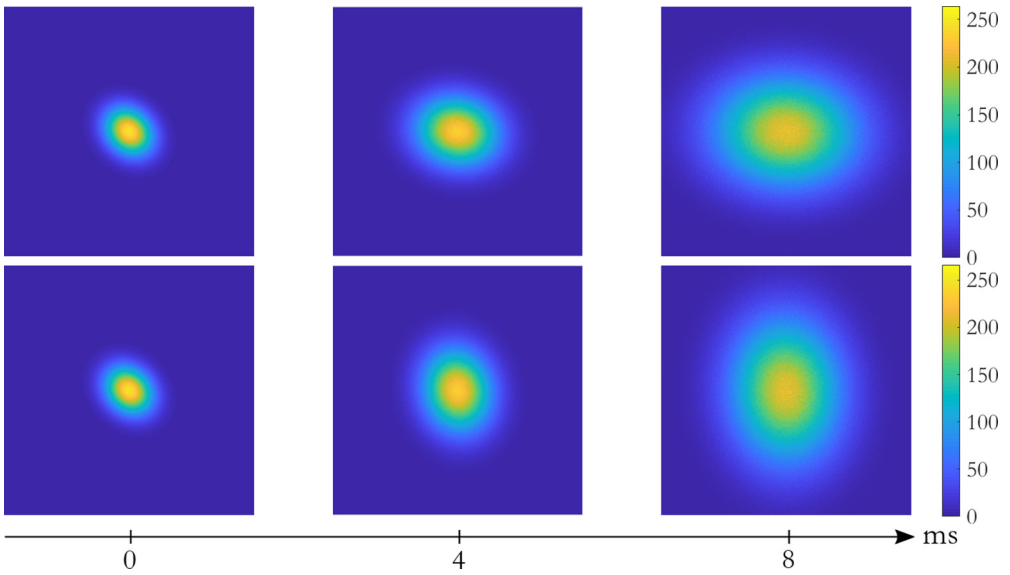

FIG. 10. Time-of-flight simulations (TOF) emphasizing the difference of behavior when reversing the rotation. The spatial density is plotted after different times of TOF for both clockwise rotation (upper) and counterclockwise rotation (lower).

clearly show a net mean rotation. Those figures were realized using a Cholesky decomposition of the covariance matrix Ξ, which gives access to (x, y, v_x, v_y) for an arbitrary number of independent particles. Here this number of atoms is chosen to be reasonably high ($n = 2 \times 10^7$) for a clear reading of the figures. Initially small, the cloud will expand and maintain an asymmetric shape, as if the rotation was rigid. Nevertheless, we keep in mind two important facts: first, the rotation is not strictly rigid due to the θ dependence in Eq. (22). Second, our model is for independent particles and thus, the optical depth has to be low such that multiple scattering, which couples atoms, can be disregarded. Finally, we note that the rotation is done in the strong overdamped limit. Indeed, the characteristic damping time of the velocity is given by m/η which is in the millisecond range, and therefore much shorter than $|\langle\omega\rangle|^{-1}$.

VI. CONCLUSION

We have shown that for a two-dimensional particle undergoing a stochastic motion with two different temperatures along perpendicular axes, and subjected to an external force deriving from a confining potential, the system evolves toward a stationary state, in which a permanent current is present when the two principal axes of the confining potential do not coincide with the temperature axes. We finally proposed to observe this phenomenon in an experiment with ultr-cold atomic gas.

ACKNOWLEDGMENTS

P.V. acknowledges Gleb Oshanin and Olivier Bénichou for fruitful discussions and the School of Physical and Mathematical Sciences, NTU, Singapore where a part of this work was done. The authors warm-heartedly acknowledge Fréderic Chevy, Dominique Delande, and Gregory Page for their careful proofreading and advice.

APPENDIX A: METHOD

We first introduce the method allowing one to obtain the complete solution of the two above models. Indeed, these models belong to the class of linear multivariate Fokker-Planck equations [32–34]. If $\mathbf{z}$ denotes an r-dimensional vector, the linear Fokker-Planck equation is then given by

$$\frac{\partial P(\mathbf{z},t)}{\partial t} = -\sum_{i,j} A_{ij} \frac{\partial z_j P(\mathbf{z},t)}{\partial y_i} + \frac{1}{2} B_{ij} \frac{\partial^2}{\partial z_i \partial z_j} P(\mathbf{z},t). \quad \text{(A1)}$$

The solution of this linear Fokker-Planck equation is a Gaussian distribution

$$P(\mathbf{z},t) = \sqrt{\frac{(2\pi)^r}{\mathrm{Det}(\Xi)}} \exp\left(-\frac{1}{2}(\mathbf{z} - \langle\mathbf{z}\rangle)^T \Xi^{-1} (\mathbf{z} - \langle\mathbf{z}\rangle)\right), \quad \text{(A2)}$$

where $\langle\cdot\rangle$ denote the average over the variable, $\mathbf{z}^T$ the transpose of $\mathbf{z}$, and $\Xi \equiv \Xi(t)$ is a time-dependent $r \times r$ covariance matrix. By taking the first and the second moments of the Fokker equation, the covariance matrix satisfies the differential equation

$$\frac{d\Xi}{dt} = A\Xi + \Xi A^T + B, \quad \text{(A3)}$$

where A and B are $r \times r$ matrices with coefficients A_{ij} and B_{ij}, respectively.

Note that for the two models defined above, the matrices A and B are symmetric. Moreover, for the sake of simplicity, one first considers the stationary solution, where the stationary covariance matrix is denoted as Ξ_s obeying to the algebraic equation

$$A\Xi_s + \Xi_s^T A = -B. \quad \text{(A4)}$$

APPENDIX B: EFFECTIVE VERLET-TYPE ALGORITHM

For the sake of simplicity, one considers a one-dimensional Langevin equation [23], but the generalization of this

algorithm in higher dimensions is straightforward. The Langevin equation is given by

$$\frac{dx}{dt} = v, \tag{B1}$$

$$m\frac{dv}{dt} = f - \eta v + \xi(t), \tag{B2}$$

where f denotes an external force, η the friction coefficient, m the particle mass, and $\xi(t)$ a Gaussian white noise [$\langle\xi(t)\rangle = 0$ and $\langle\xi(t)\xi(t')\rangle = 2\eta T\delta(t-t')$, T is the bath temperature and $\delta(t)$ the Dirac function]. Integrating the above equations over a time step dt, one obtains

$$x_{n+1} = x_n + \int_{t_n}^{t_{n+1}} v(t')dt', \tag{B3}$$

$$m(v_{n+1} - v_n) = \int_{t_n}^{t_{n+1}} f\,dt' - \eta(x_{n+1} - x_n) + R_{n+1}, \tag{B4}$$

where $x_n, v_n, x_{n+1}, v_{n+1}$ denote the positions and velocities at times t_n and $t_{n+1} = t_n + dt$, respectively. R_{n+1} is a Gaussian random number such that $\langle R_i\rangle = 0$ and $\langle R_i R_j\rangle = 2\eta T\,dt\,\delta_{ij}$.

Approximating $\int_{t_n}^{t_{n+1}} v(t')dt' \simeq \frac{dt}{2}(v_{n+1} + v_n)$, and inserting Eq. (B4) into Eq. (B3), one obtains

$$x_{n+1} = x_n + b\,dt\left(v_n + \frac{1}{2m}\left[\int_{t_n}^{t_{n+1}} f\,dt' + R_{n+1}\right]\right), \tag{B5}$$

with

$$b = \left(1 + \frac{\eta dt}{2m}\right)^{-1}. \tag{B6}$$

Performing a second-order expansion of the integral of the deterministic force, the equations of motion become

$$x_{n+1} = x_n + b\,dt\left(v_n + \frac{dt}{2m}f_n + R_{n+1}\right), \tag{B7}$$

$$v_{n+1} = v_n + \frac{dt}{2m}(f_n + f_{n+1}) - \frac{\eta}{m}(x_{n+1} - x_n) + \frac{1}{m}R_{n+1}. \tag{B8}$$

Finally, by inserting Eq. (B7) into Eq. (B8), the discretized equation of velocity is then given by

$$v_{n+1} = a v_n + \frac{dt}{2m}(a f_n + f_{n+1}) + \frac{b}{m}R_{n+1}, \tag{B9}$$

with

$$a = \left(1 - \frac{\eta dt}{2m}\right)b. \tag{B10}$$

[1] B. Derrida and E. Brunet, *Einstein Aujourd'hui* (EDP Sciences, Les Ulis, 2005), p. 205.
[2] P. Visco, J. Stat. Mech. (2006) P06006.
[3] H. C. Fogedby and A. Imparato, J. Stat. Mech. (2011) P05015.
[4] H. C. Fogedby and A. Imparato, J. Stat. Mech. (2014) P11011.
[5] C. Van den Broeck, R. Kawai, and P. Meurs, Phys. Rev. Lett. **93**, 090601 (2004).
[6] C. V. den Broeck, P. Meurs, and R. Kawai, New J. Phys. **7**, 10 (2005).
[7] P. Reimann, Phys. Rep. **361**, 57 (2002).
[8] Y. Murashita and M. Esposito, Phys. Rev. E **94**, 062148 (2016).
[9] S. Ciliberto, A. Imparato, A. Naert, and M. Tanase, J. Stat. Mech. (2013) P12014.
[10] S. Ciliberto, A. Imparato, A. Naert, and M. Tanase, Phys. Rev. Lett. **110**, 180601 (2013).
[11] A. Bérut, A. Petrosyan, and S. Ciliberto, Europhys. Lett. **107**, 60004 (2014).
[12] A. Bérut, A. Imparato, A. Petrosyan, and S. Ciliberto, Phys. Rev. Lett. **116**, 068301 (2016).
[13] H. C. Fogedby and A. Imparato, Europhys. Lett. **119**, 50007 (2017).
[14] S. Ciliberto, Phys. Rev. X **7**, 021051 (2017).
[15] A. Argun, J. Soni, L. Dabelow, S. Bo, G. Pesce, R. Eichhorn, and G. Volpe, Phys. Rev. E **96**, 052106 (2017).
[16] K.-H. Chiang, C.-L. Lee, P.-Y. Lai, and Y.-F. Chen, Phys. Rev. E **96**, 032123 (2017).
[17] A. Ryabov, V. Holubec, M. H. Yaghoubi, M. Varga, M. E. Foulaadvand, and P. Chvosta, J. Stat. Mech. (2016) 093202.
[18] V. Holubec, A. Ryabov, M. H. Yaghoubi, M. Varga, A. Khodaee, M. E. Foulaadvand, and P. Chvosta, Entropy **19**, 119 (2017).
[19] R. Filliger and P. Reimann, Phys. Rev. Lett. **99**, 230602 (2007).
[20] V. Dotsenko, A. Maciołek, O. Vasilyev, and G. Oshanin, Phys. Rev. E **87**, 062130 (2013).
[21] U. Seifert, Rep. Prog. Phys. **75**, 126001 (2012).
[22] A. Crisanti, A. Puglisi, and D. Villamaina, Phys. Rev. E **85**, 061127 (2012).
[23] N. Gronbech-Jensen and O. Farago, Mol. Phys. **111**, 983 (2013).
[24] D. W. Sesko, T. G. Walker, and C. E. Wieman, J. Opt. Soc. Am. B **8**, 946 (1991).
[25] T. Walker, D. Hoffmann, P. Feng, and R. Williamson, Phys. Lett. A **163**, 309 (1992).
[26] T. Dubcek, N. Santic, D. Jukic, D. Aumiler, T. Ban, and H. Buljan, Phys. Rev. A **89**, 063415 (2014).
[27] N. Santic, T. Dubcek, D. Aumiler, H. Buljan, and T. Ban, Sci. Rep. **5**, 13485 (2015).
[28] N. Santic, T. Dubcek, D. Aumiler, H. Buljan, and T. Ban, J. Opt. Soc. Am. B **34**, 1264 (2017).
[29] S. Stenholm, Rev. Mod. Phys. **58**, 699 (1986).
[30] H. Katori, T. Ido, Y. Isoya, and M. Kuwata-Gonokami, Phys. Rev. Lett. **82**, 1116 (1999).
[31] M. Chalony, A. Kastberg, B. Klappauf, and D. Wilkowski, Phys. Rev. Lett. **107**, 243002 (2011).
[32] N. Van Kampen, *Stochastic Processes in Physics and Chemistry* (Elsevier Science, Amsterdam, 1992).
[33] M. Lax, Rev. Mod. Phys. **32**, 25 (1960).
[34] C. Gardiner, *Stochastic Methods: A Handbook for the Natural and Social Sciences*, Springer Series in Synergetics (Springer, Berlin/Heidelberg, 2009).